J. Fluid Mech. (1975), *vol.* 72, *part* 1, *pp.* 49–65
Printed in Great Britain

Boundary layer over a blunt body at low incidence with circumferential reversed flow

By K. C. WANG
Martin Marietta Laboratories, Baltimore, Maryland 21227

(Received 2 December 1974)

This paper investigates the three-dimensional laminar boundary layer over a blunt body (a prolate spheroid) at low incidence and with reversed flow. Results reflecting the general characteristics of such a problem are presented. More significant are the features relating to the circumferential flow reversal. Some of these features confirm our early hypotheses concerning the existence of a reversed region ahead of separation and the role of the zero-$c_{f\theta}$ line in the general context of separation in three dimensions. Other features are unexpected, including the distribution of $c_{f\mu}$ and the shape of the separation line. Here $c_{f\theta}$ and $c_{f\mu}$ denote, respectively, the circumferential and meridional components of the skin friction.

1. Introduction

This work is a continuation of two earlier papers (Wang 1974*a*, *b*) and is concerned with the three-dimensional laminar boundary layer over a blunt body (i.e. a prolate spheroid; see figure 1) at low incidence with circumferential reversed flow. The two earlier papers dealt with the same problem at high incidence and at extremely high incidence respectively, but did not touch upon such reversed flow.

In the usual steady two-dimensional boundary-layer theory, calculation of reversed flow has been forbidden because it is against the initial-value idea of the governing parabolic system of equations. Although Catherall & Mangler's (1966) work has sometimes been considered an exception to this rule, this is not the case because they did not follow the usual procedure.

Investigation of such reversed flow was prompted by the following sequence of developments. First, our symmetry-plane boundary-layer study (Wang 1970) indicated that circumferential flow reversal always occurs before meridional flow reversal for an elongated prolate spheroid at incidence. The situation is illustrated in figure 2 by points R and S, which signify, respectively, the onset of reversal of the circumferential and meridional flows.

Later, in studying the separation criteria in three dimensions (Wang 1972), it was hypothesized that the aforementioned reversal of the circumferential flow may or may not signify separation depending on whether or not an envelope of the limiting streamlines is formed immediately after such a reversal (figure 2). On the basis of this criterion, the circumferential reversed flow at high and

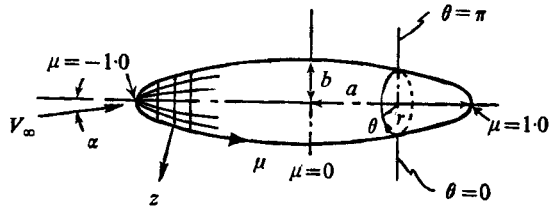

FIGURE 1. Prolate spheroid, co-ordinates and notation.

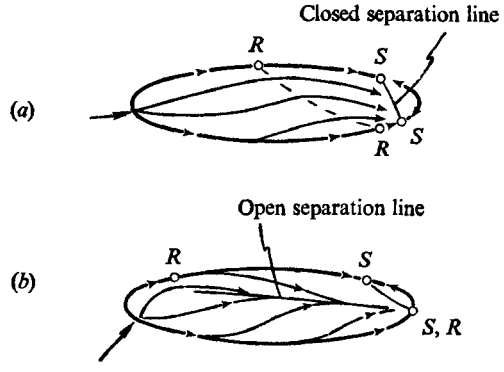

FIGURE 2. Separation patterns. (*a*) Low incidence. (*b*) High incidence.

extremely high incidences was considered as separated flow; reversed flow at low incidence remains part of the boundary-layer flow. Once this low incidence flow is accepted as part of the boundary layer, it must be calculated in an initial-value manner.

At first, calculation of such circumferential reversed flow raised conceptual questions: can such a problem still be dealt with as an initial-value problem? Is it still 'well posed'? Lack of a theoretical basis made it quite difficult to arrive at clear answers.

However, the question of the problem's being 'well posed' has since been gradually rationalized by using the concept of the zones of influence and dependence for three-dimensional boundary layers. So long as this dependence rule is satisfied, calculation can be continued regardless of whether or not reversal occurs in either the circumferential or meridional component of the flow (but not both). This idea is valid because reversal of one component of the flow is not the same as reversal of the resultant flow; hence it does not violate the initial-value idea. In fact, the flow direction (parallel to the body surface) varies across the three-dimensional boundary layer at a given point on the body surface, thus sweeping out a certain solid angle. A distinctive, single resultant flow direction does not exist in this case. The dependence rule, which requires the computation mesh to enclose the solid angle, ensures precisely the satisfaction of the initial-value concept.

Confusion regarding the ability to calculate circumferential flow reversal arose also in recent years in the related problem of the boundary layer over a

spinning supersonic pointed cone. In that problem, the reversal is caused by spinning motion. In our present problem, on the other hand, the reversal is self-induced. Apart from this difference, the logic of the approach is the same for both. Dwyer (1971) and Lin & Rubin (1973) reported that the spinning-cone problem could not be treated as an initial-value boundary-layer problem; but later Dwyer (1974) reversed this position. Without going into details of this problem (see Wang 1975), it suffices for our purpose here to point out that the mere fact of such confusion attests to the unconventional nature of our problem.

In the present work, we describe our method of solution and the calculated results. Apart from those providing a general picture of the boundary layer over a blunt body of revolution at low incidence, the most important results are those relating to the aforementioned circumferential flow reversal and its consequences. Some of the results confirmed our early hypotheses about the existence of a reversed region ahead of separation and the role of the zero-$c_{f\theta}$ line in the general context of separation in three dimensions. Other results are somewhat unexpected, including the distribution of the meridional skin friction inside the reversed region (§3.4) and the shape of the separation line (§3.5).

We also proposed earlier (Wang 1972) a separation cycle varying with incidence: namely, for a not-too-blunt body, the separation is of a closed or bubble type at low incidence (figure 2), of an open (or free vortex layer) type at high incidence and of a closed type again at extremely high incidence. Previous full three-dimensional boundary-layer calculations for high and extremely high incidence (Wang 1974*a*, *b*) and the present work for low incidence confirm these ideas. Recent extensive surface-flow experiments (Zakkay, Miyazawa & Wang 1974) on blunt cones and a space shuttle orbiter model provide further support for these ideas on an open *vs.* a closed separation.

The boundary layer over a slender body of revolution at small incidence with a circumferential reversed flow was investigated by Nonweiler (1955, 1970). The linearized perturbation approach to the boundary-layer equations and the inviscid slender-body theory used impose severe limitations on the significance of his results. Nevertheless, some comparisons with his cross-plane flow patterns are given in §3.3.

Early investigations on the boundary layer over a spheroid at small incidence were made in the 1950s by several authors (for example, Eichelbrenner & Oudart 1955; Zatt 1956). Approximate methods such as the integral method, independence principle, etc., were used; however, these studies are now mainly of historical interest.

2. Equations and method of solution

The governing equations and general methods of solution were outlined earlier (Wang 1974*a*). Here we briefly recapitulate the definition of the symbols used and then discuss the aspects of the method of solution which specifically apply to the low incidence case and the reversed flow involved.

2.1. *Definition of symbols*

Referring to figure 1, α is the incidence angle, μ and θ are two surface co-ordinates along the meridional and circumferential directions, respectively, and z denotes the normal co-ordinate. The metric coefficients for the co-ordinates μ and θ are h_μ and h_θ. e is the eccentricity. a and b are the semi-major and semi-minor axes. (u, v, w) are the velocities along the (μ, θ, z) directions; u and v are non-dimensionalized with the flow velocity V_∞ at infinity, w with $V_\infty/R^{\frac{1}{2}}$, where $R\,(= V_\infty a/\nu)$ is the Reynolds number, and z with $a/R^{\frac{1}{2}}$. p is the pressure non-dimensionalized with ρV_∞^2, where ρ is the density. U and V are the inviscid velocities at the boundary-layer edge. In the present case of a prolate spheroid, U and V, and hence the pressure p, are known from an exact inviscid flow solution.

The meridional component of the skin friction is defined by

$$c_{f\mu} = R^{-\frac{1}{2}}(\partial u/\partial z)_{z\to 0}, \tag{1}$$

with the circumferential component $c_{f\theta}$ defined similarly. The limiting streamlines (also called the skin-friction lines) are determined from

$$\frac{h_\mu d\mu}{h_\theta d\theta} = \frac{(\partial u/\partial z)_{z\to 0}}{(\partial v/\partial z)_{z\to 0}} = \frac{c_{f\mu}}{c_{f\theta}}. \tag{2}$$

The meridional component Δ_μ^* of the displacement thickness, based on the u-velocity profiles, is defined by

$$\Delta_\mu^* = \frac{U}{q}\int_0^\infty (1 - u/U)\,dz, \tag{3}$$

where q is the total inviscid velocity:

$$q = (U^2 + V^2)^{\frac{1}{2}}. \tag{3a}$$

The circumferential component Δ_θ^* is defined similarly.

2.2. *Method of solution*

Computation schemes. Our method is an implicit finite-difference method of the Crank–Nicolson type and was employed in a body-fixed co-ordinate system. Several computation meshes (figure 3) were used to fulfil the conditions regarding the zones of influence and dependence for different regions of the body surface. For convenience, these meshes are designated as schemes 1, 2, 3, 4(*a*) and 4(*b*). Scheme 1 employs a one-step mesh (figure 3*a*) applicable to an area where no reversal occurs in either surface component of the flow. Schemes 2, 4(*a*) and 4(*b*) (figures 3*b*, *d* and *e*) are for cases where the circumferential flow reverses. In all schemes, station 4 is to be calculated from known stations 1–3 and 5. The shaded area denotes the possible zone of dependence for station 4. The normal direction (to the body) is not shown in these figures. Scheme 3 (figure 3*c*) applies where the meridional flow may reverse; it was not used in the present low incidence calculation and is shown here only for reference. It is clear that schemes 2 and 3 (figures 3*b*, *c*) are variations of each other, as are schemes 4(*a*) (Krause 1969)

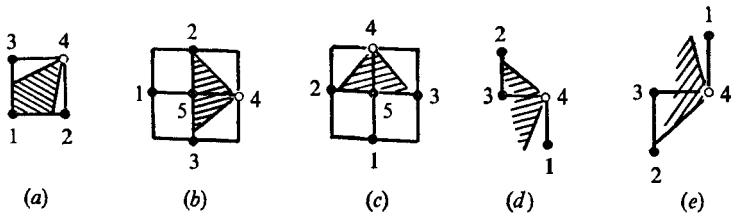

FIGURE 3. Computation meshes. (*a*) Scheme 1. (*b*) Scheme 2. (*c*) Scheme 3. (*d*) Scheme 4(*a*). (*e*) Scheme 4(*b*).

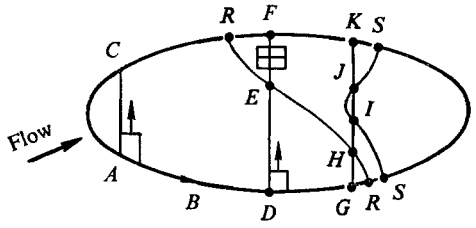

FIGURE 4. Computational procedure.

and 4(*b*) (figures 3*d*, *e*). Schemes 4(*a*) and (*b*) cover larger zones of dependence than does scheme 2 and hence are preferred. But scheme 2 (figure 3*b*) does not require known station(s) on the vertical co-ordinate line passing through station 4, a useful advantage under certain circumstances. Similarly, scheme 3 does not require known station(s) on the horizontal co-ordinate line through station 4.

Computational procedure. At low incidence, the flow profiles near the front vertex do not vary significantly, and the more complicated starting procedure developed for high incidences (Wang 1974*a*, *b*) was not needed. Instead, the boundary-layer calculation was started using the stagnation-region profiles all along *AC* (figure 4), with simple modifications to match the local outer-edge velocities. The solution along *AB* was obtained from a separate symmetry-plane boundary-layer calculation. With initial values along *AC* and *AB* thus obtained, computation proceeded from the windward side towards the lee side along succeeding parallels using scheme 1 until circumferential flow reversal started. When reversal occurred near a mid-section such as *DEF* (figure 4), scheme 1 was used from *D* to *E* and scheme 2 from *E* to *F*, although the whole line may be calculated by scheme 4(*a*) alone if preferred. Shortly before separation, calculation cannot proceed all the way from the windward to the lee side. Referring to section *GHIJK* in figure 4, scheme 1 was used from *G* to *H* and scheme 2 from *H* to *I*. Between *I* and *J*, no solution was obtained. The upper part *JK* was calculated downward from *K* to *J*, using scheme 4(*b*) with the lee-side symmetry-plane boundary-layer solution providing some of the initial values.

Difference approximation. The difference approximations for schemes 1 and 3 have been described before (Wang 1974*a*). Scheme 2 is analogous to scheme 3 with an interchange of the roles of the two surface co-ordinates. The difference equations can readily be written down. The only important modification to prior work (Wang 1974*a*) concerns the calculation of w from the continuity equation.

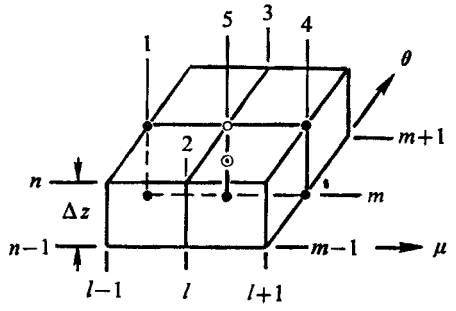

FIGURE 5. Difference approximation of w for scheme 2.

Following Wang (1974*a*), the derivative $\partial w/\partial z$ for scheme 2 would be replaced by

$$\partial w/\partial z = (2\Delta z)^{-1}(w_{l+1,m,n} - w_{l+1,m,n-1} + w_{l-1,m,n} - w_{l-1,m,n-1}),$$

which is an average of values at stations 1 and 4. w is calculated at station 4, as were u and v. A simpler alternative approximation is

$$\partial w/\partial z = (\Delta z)^{-1}(w_{l,m,n} - w_{l,m,n-1}),$$

which involves values of w at station 5 only. Thus w is calculated at station 5, though u and v are calculated at station 4. (See figure 5.)

In our calculations, numerical values of w are an order of magnitude larger than those of u and v. The value of w is most sensitive to any fluctuation or inaccuracy during the computation and also varies much more (numerically) from point to point on the body surface. When the original approximation was used, results for w gradually exhibited signs of fluctuation after some distance downstream (100 stations), eventually becoming anomalous, and the computation broke down. Similar difficulty with w was also found later by Kitchens, Gerber & Sedney (1975). If more than two stations (e.g. stations 1–4) are used in approximating $\partial w/\partial z$ on the assumption that more stations would yield better approximation, the situation worsens in that w fluctuates sooner. On the other hand, in the alternative approximation, since only values of w at a single central station 5 are involved, fluctuation due to the differences between the values of w at neighbouring stations is eliminated, and the aforementioned difficulty does not occur.

We point out that the same difficulty was experienced in our earlier development of scheme 1 (Wang 1974*a*). At first, the average over four corner stations (figure 3*a*) was used in calculating w and difficulties similar to those experienced with scheme 2 were observed. Then an approximation similar to the alternative one was applied at the central point (figure 3*a*) to resolve the problem. Conventional numerical stability analysis is applied to the linearized version of the momentum difference equations and therefore does not provide insight into the difficulty under discussion, which comes from the continuity equation. Schemes 4(*a*) and (*b*) have been developed primarily for the spinning-body problem and are described elsewhere (Wang 1975).

Schemes 2 and 4(*a*) of the present calculation were tested against an exact

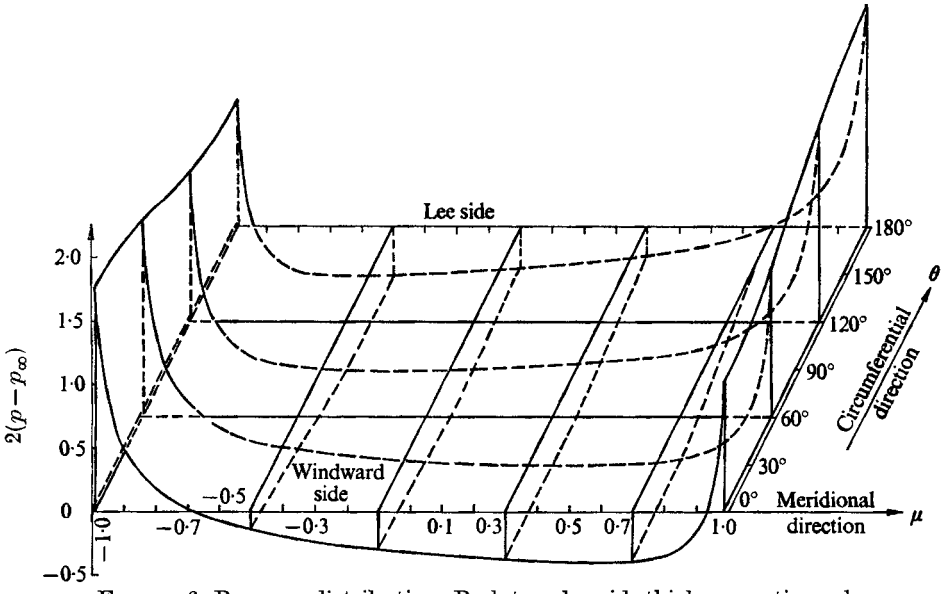

FIGURE 6. Pressure distribution. Prolate spheroid, thickness ratio = $\frac{1}{4}$, incidence angle = 6°.

similarity solution and against scheme 1, developed earlier, under conditions wherein all these schemes are valid. A similarity test of and check on scheme 1 were reported earlier (Wang 1974*a*).

3. Results and discussion

3.1. *Inviscid input*

The results shown below are for a prolate spheroid having a minor/major axis ratio of $\frac{1}{4}$ at an incidence of 6°. An exact inviscid solution for the present problem is available from standard hydrodynamics texts. Figure 6 gives the theoretical pressure distribution over the body which, at low incidence, is valid for the present boundary-layer investigation. The pressure distribution is generally favourable; at worst it may be gently adverse on the lee side of the afterbody (except near the rear end). The pressure varies very little in the circumferential direction. The inviscid circumferential velocity V is an order of magnitude smaller than the inviscid meridional velocity U, a reflexion of the dominance of the latter component of the flow at low incidence. The variation of U is small in the meridional direction and almost imperceptible in the circumferential direction except near the two ends. V is constant for a prolate spheroid along the meridians and varies sinusoidally along the parallels.

3.2. *Boundary-layer profiles*

Figures 7(*a*)–(*d*) present boundary-layer velocity profiles along circumferential sections. Figure 7(*a*) shows that, along $\mu = -0{\cdot}5$, the u and v profiles both slowly grow steeper and thicker from the windward towards the lee side. This pattern of variation of the profiles is quite typical for the front of the body. Close to the

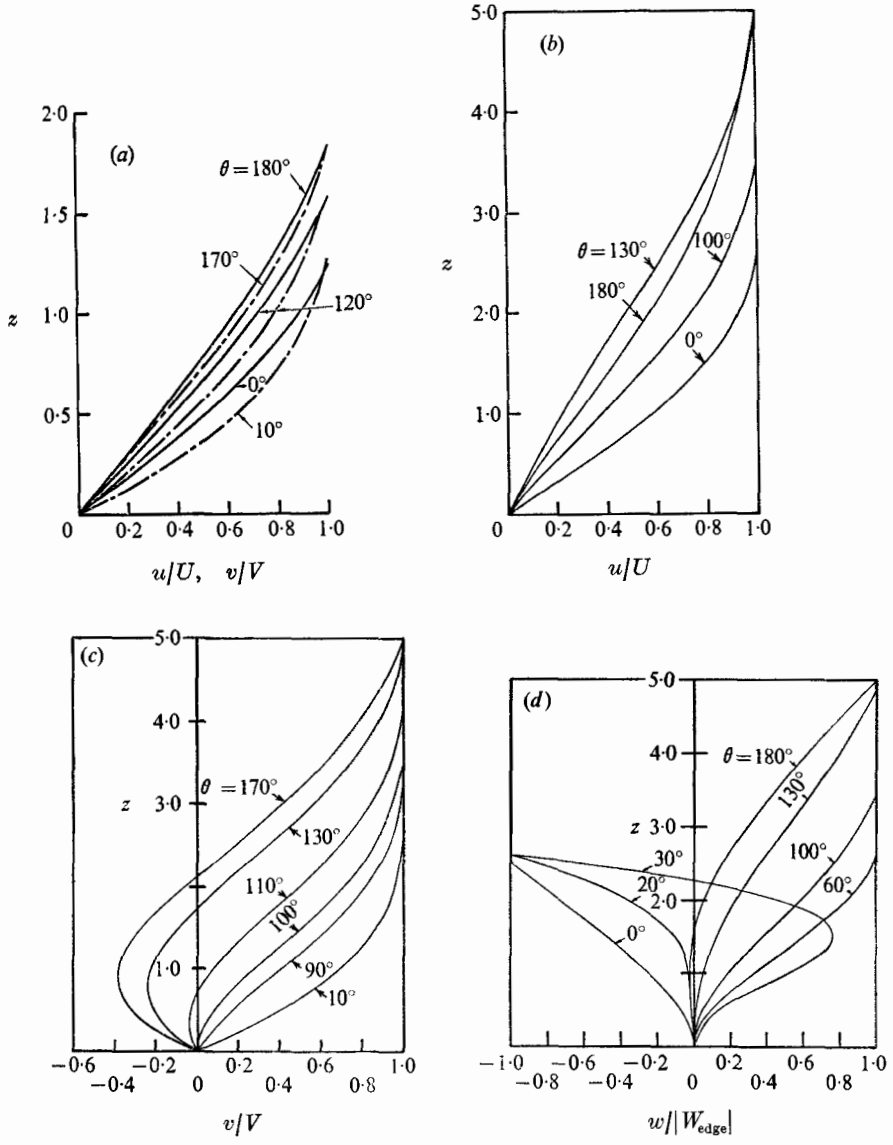

FIGURE 7. Velocity profiles. (*a*) $\mu = -0{\cdot}5$: ——, u/U; — – —, v/V. (*b*)–(*d*) $\mu = 0{\cdot}365$.

mid-section, $\mu = 0$, the v profile begins to steepen rapidly, so that reversed circumferential flow begins near the lee-side symmetry plane.

Further downstream, over the afterbody, such reversed flow becomes more pronounced (figure 7*c*) and causes the meridional flow u to vary in a different way. This is illustrated in figure 7(*b*). Along $\mu = 0{\cdot}365$, starting from the windward symmetry plane $\theta = 0$, the u profile changes very little before entering the reversed-flow region around $\theta = 100°$. Once inside the reversed-flow region, the u profile steepens much more rapidly between $\theta = 100°$ and 130°, this being accompanied by a relatively quick decrease in the meridional skin friction (see

figure 11*b*). Above 130°, this trend is reversed and the u profile flattens down such that the meridional skin friction increases from $\theta = 130°$ to $\theta = 180°$. Thus the reversal of the v profile changes considerably the variation of the u profile. Before the reversed flow starts (figure 7*a*), the u profile consistently steepens from $\theta = 0$ to 180°.

A typical w profile over the front of the body is negative (i.e. pointing towards the body) over the windward and positive (i.e. pointing away from the body) over the lee side. The change from negative to positive takes place at smaller θ as μ increases. At $\mu = 0{\cdot}50$, for example, this change occurs between $\theta = 80°$ and 90°, starting from the part near the body. Typical w profiles over the afterbody when the circumferential flow reverses are shown in figure 7 (*d*) for $\mu = 0{\cdot}365$. Between $\theta = 0$ and 20°, w is negative. At $\theta = 30°$, w becomes positive near the body, but remains negative close to the outer edge. As θ increases further, w becomes entirely positive. Beyond $\theta = 140°$, the behaviour is opposite to that at $\theta = 30°$, i.e. w is negative near the body, but remains positive in the outer layer.

Still further downstream, say at $\mu = 0{\cdot}64$, calculation could be continued only from $\theta = 0$ to about 82°, where the meridional skin friction vanishes and the u profile starts to show reversal along with the v profile. When both profiles reverse, the problem ceases to be an initial-value boundary-layer problem.

The upper portion of the calculation along $\mu = 0{\cdot}64$ was completed by another procedure. It started from $\theta = 180°$, proceeding downward, and stopped at $\theta = 110°$, when the meridional skin friction decreased to a vanishingly small value, thus leaving the middle portion between 80° and 110° undetermined. Profiles from this part of the calculation show the same pattern as in figure 7 (*b*), i.e. the u profile moves down (rather than up) as θ increases from 110° to 180°.

3.3. *Cross-plane flow pattern*

The flow direction in a cross-plane (i.e. at a fixed μ station or a plane perpendicular to the major axis) is represented by arrows in figure 8. The direction is given by $\tan^{-1}(h_\theta w/v)$ and is presented in θ, z co-ordinates. The solid curves drawn therefrom represent the cross-plane streamlines. Along $\mu = 0{\cdot}365$, a pattern indicating inflow (i.e. towards the body surface) between $\theta = 0$ and 30° gradually changes into one indicating outflow (i.e. away from the body surface) above 30°. At the lower right corner of figure 8 a fairly large reversed-flow region occurs.

The cross-plane flow pattern shown in figure 8 may be redrawn around a semicircular cross-section to give a more physical picture. Further reduction of similar patterns (with the arrows omitted) results in the sequence shown in figures 9 (*a*)–(*e*), where the increase in the boundary-layer thickness around the body has not been taken into account. Figures 9 (*a*) and (*b*) show how, over the forebody, an inflow pattern over the whole cross-plane at $\mu = -0{\cdot}95$ changes gradually into a mixed inflow and outflow pattern at $\mu = -0{\cdot}60$. Figure 9 (*c*) ($\mu = 0{\cdot}11$) indicates the onset of the reversed region. The downstream growth of the reversed region is shown in figure 9 (*d*). Figure 9 (*e*) shows the windward- and lee-side boundary layers separated by an opening to signify the uncalculated separated-flow region.

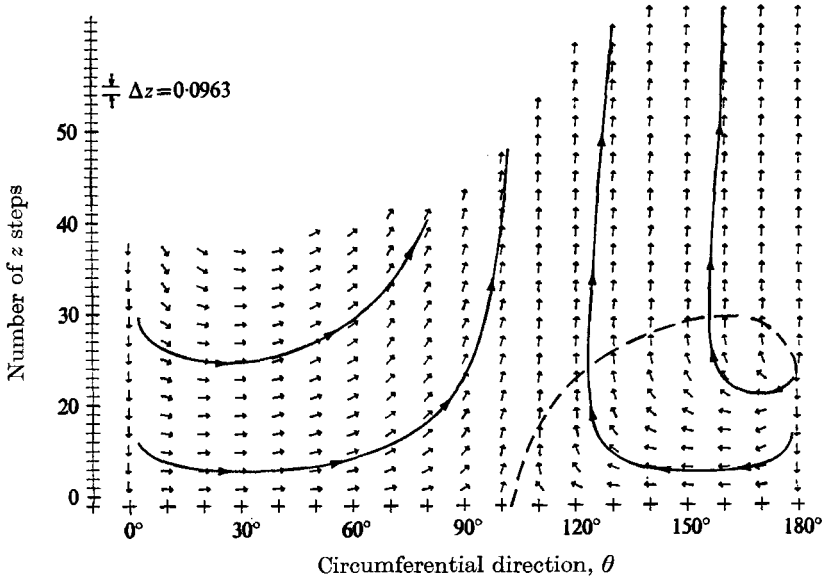

FIGURE 8. Cross-plane flow pattern. $\mu = 0{\cdot}365$.

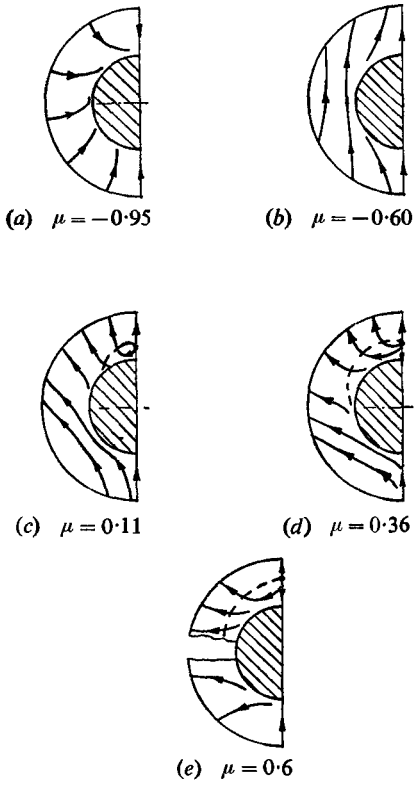

FIGURE 9. Cross-plane flow pattern.

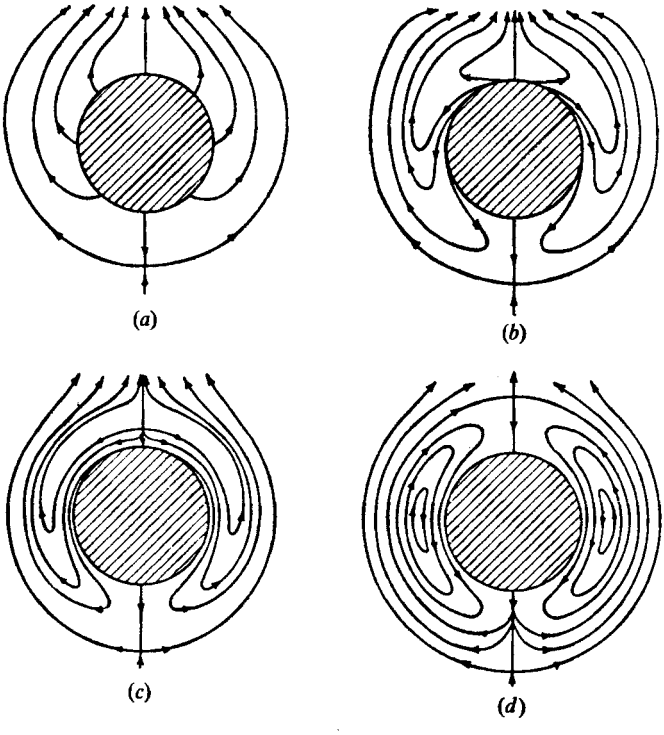

FIGURE 10. Nonweiler's cross-plane flow patterns.

Cross-plane flow patterns were also presented (figures 10*a–d*) by Nonweiler (1955, 1970), on the basis of his linearized boundary-layer analysis for a slender body of revolution at small incidence. Figure 10(*a*) indicates that, over the front of the body, there is no reversed flow. Further downstream reversal of the circumferential flow does appear (figure 10*b*) and grows in extent (figures 10*c*, *d*).

Both agreement and differences are noted between our version of the cross-plane flow patterns and Nonweiler's. Over the front, we predict an overwhelmingly inflow pattern (figures 9*a*, *b*). Nonweiler envisions a completely outflow pattern (figure 10*a*). Further downstream, both versions exhibit a circumferential reversed flow, but Nonweiler pictures a closed vortex pattern (figure 10*b*), while our results do not reveal the same behaviour (figures 9*c*, *d*). This difference apparently arises because the z co-ordinate and the w velocity calculated are on the stretched boundary-layer scale, while Nonweiler's sketches might have been made with the physical scale in mind. These two scales differ by a factor of $\sqrt{R}$. Still further downstream, Nonweiler's version indicates that the vortex pattern persists and extends around the body (figures 10*c*, *d*). Our results predict that the windward- and lee-side boundary layer are partitioned by a separated flow region (figure 9*e*). It is not clear whether these differences are due to the fact that the body shape considered by Nonweiler is more slender than ours.

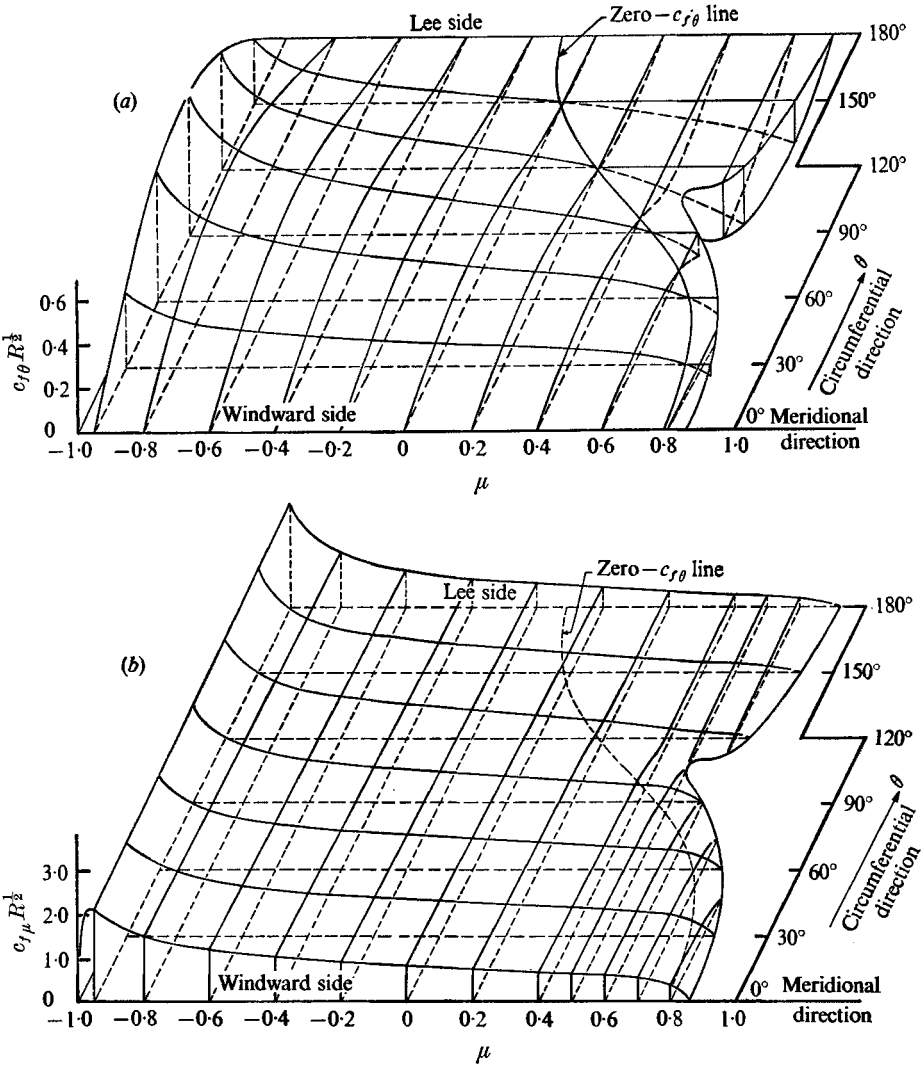

FIGURE 11. (*a*) Circumferential skin friction $c_{f\theta}$. (*b*) Meridional skin friction $c_{f\mu}$. Prolate spheroid, thickness ratio = $\frac{1}{4}$, incidence angle = 6°.

3.4. *Skin friction*

Figure 11(*a*) gives the distribution of the circumferential skin friction $c_{f\theta}$ over the body. Along the meridional direction, $c_{f\theta}$ slowly decreases from positive values over the forebody to negative values over the afterbody. Remember that, in the present problem, the inviscid velocity V is constant along meridians, hence the meridional variation of $c_{f\theta}$ is free from any contribution from a corresponding inviscid flow gradient, i.e. $\partial V/\partial\mu$. In the circumferential direction, $c_{f\theta}$ increases over the forebody from zero at $\theta = 0$ to a maximum value in the middle and then decreases to zero at $\theta = 180°$, following the general pattern of V, which varies as $\sin\theta$. Over the afterbody, $c_{f\theta}$ becomes negative on the lee side. The zero-$c_{f\theta}$ line, along which $c_{f\theta}$ vanishes, segregates the reversed-flow region from the front regular boundary-layer region.

Figure 11(*b*) shows the distribution of the meridional skin friction $c_{f\mu}$ over the body. $c_{f\mu}$ is an order of magnitude larger than $c_{f\theta}$, which reflects the dominance of the meridional component of the flow. Over most of the body, $c_{f\mu}$ gradually decreases along meridians from the front towards the rear and along parallels from the windward towards the lee side. This low incidence pattern provides an interesting contrast to those presented previously for higher incidences (Wang 1974*a*, *b*). The zero-$c_{f\theta}$ line is superposed in figure 11(*b*) to indicate clearly where the reversed-flow region starts. The pattern of the $c_{f\mu}$ distribution inside the reversed region is particularly interesting because it exhibits the effect of circumferential flow reversal upon the meridional flow and because of its direct connexion with the separation pattern, to be discussed next. Along $\mu = 0{\cdot}40$ in figure 11(*b*), $c_{f\mu}$ maintains the trend of a gradual decrease from $\theta = 0$ over the windward surface; upon entering the reversed region, the drop in $c_{f\mu}$ is relatively sharper (as $c_{f\theta}$ increases negatively) between $\theta = 110°$ and 120°; from 120° to 180°, $c_{f\mu}$ changes from decreasing to increasing (as $c_{f\theta}$ increases from a negative value to zero). Along $\mu = 0{\cdot}50$ and $0{\cdot}6$, $c_{f\mu}$ becomes zero near $\theta = 100°$, and between 100° and 110°, no boundary-layer solution was found.

Inside the reversed region, $c_{f\mu}$ has an opposite trend, increasing instead of decreasing towards $\theta = 180°$. This is accompanied by the flattening of the u profile discussed before and occurs on the lee side of the afterbody, where an adverse pressure distribution prevails. Adverse pressure distributions generally tend to steepen a profile rather than flatten it. Apparently this unusual behaviour is attributable to the reversal of the circumferential flow.

The increase in $c_{f\mu}$ under adverse pressure conditions was first noticed in our previous symmetry-plane boundary-layer calculation (Wang 1970). However, it was found only at higher incidences, and the increase was in the downstream meridional direction, rather than in the circumferential direction noted here.

3.5. *Limiting flow pattern and separation*

In figure 12(*a*), the arrows indicate the local limiting flow direction determined according to (2). The solid lines drawn on the basis of these arrows represent the limiting streamlines. The zero-$c_{f\theta}$ line is again superposed. In the present, low incidence case, the limiting flow does not turn sharply upon crossing the zero-$c_{f\theta}$ line, hence no envelope of those limiting streamlines is formed immediately behind. Although the zero-$c_{f\theta}$ line can be closely approximated as the separation line at higher incidences, the same line has little to do with separation at low incidence. Across the zero-$c_{f\theta}$ line, the limiting streamlines merely start to bend downwards. This proposition was one of the basic conjectures in our earlier proposed separation criteria (Wang 1972); it is confirmed now by the full three-dimensional calculation.

The limiting flow is presented in especially great detail inside the reversed region up to separation. By virtue of the unexpected behaviour of $c_{f\mu}$ (i.e. it vanishes and presumably becomes negative in the middle along the circumferential direction), the resulting shape of the separation line is rather unexpected, and is of the closed type according to our classification mentioned in the introduction. As in previous, higher incidence cases, the separation line is determined

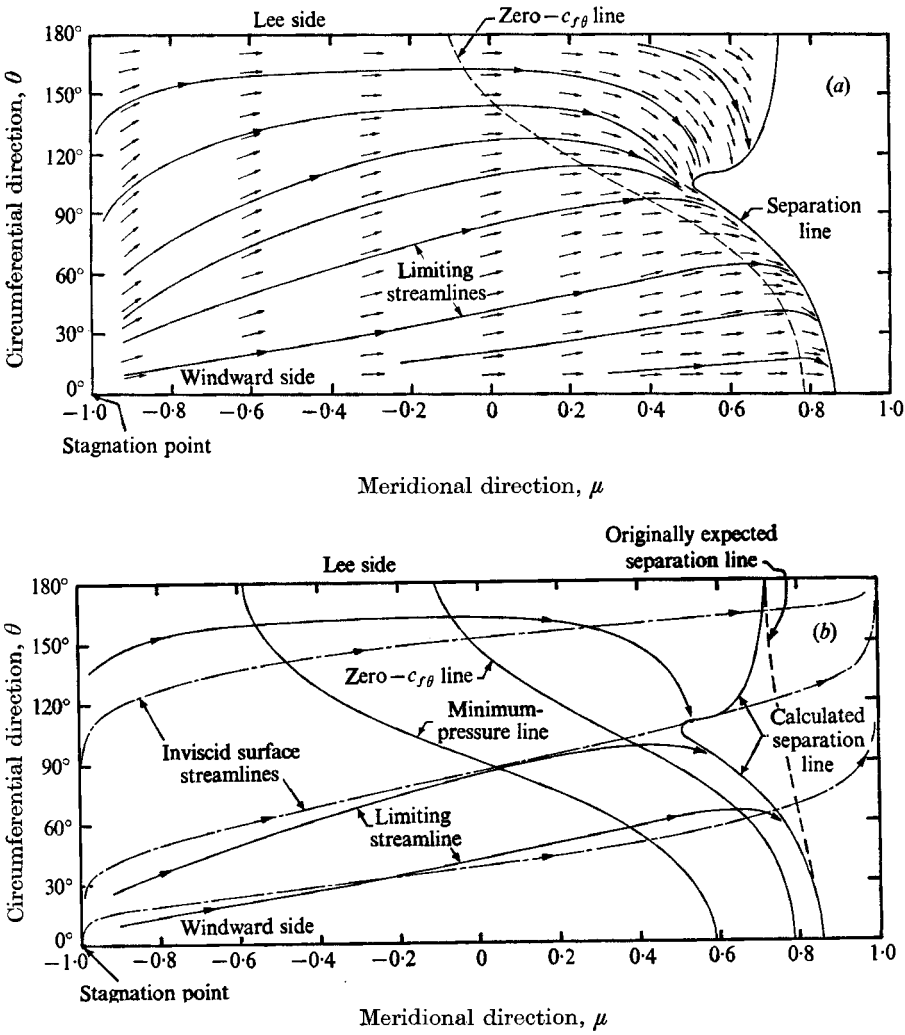

FIGURE 12. (*a*) Limiting streamlines and separation line. (*b*) Comparisons. Prolate spheroid, thickness ratio = $\frac{1}{4}$, incidence angle = 6°.

by following the definition of a separation line as an envelope of the limiting streamlines. But here the separation line can also closely be identified as the zero-$c_{f\mu}$ line. Since the separation occurs inside the circumferential reversed region, the vanishing of $c_{f\mu}$ would terminate the boundary-layer calculation from considerations of both violation of the basic idea of an initial-value problem and the computational difficulties experienced.

The calculated separation line thus obtained differs from the originally expected one, which was assumed, purely by intuition, to be a line (see figure 12*b*) more or less directly connecting the points of zero meridional skin friction on the windward- and lee-side symmetry planes.

In figure 12(*b*) the limiting streamlines and separation line are superposed on the minimum-pressure line and the inviscid surface streamlines. Along the

minimum-pressure line, the pressure gradients in both the meridional and circumferential direction vanish. Above this line, both gradients are positive and adverse. Below this line, both gradients are negative and favourable. Following the minimum-pressure line is the zero-$c_{f\theta}$ line, and then the separation line. The distinction between the inviscid streamlines and the limiting streamlines is especially drastic in the lee-side reversed region. The inviscid flow points upwards; the limiting flow turns downwards.

3.6. *Displacement thicknesses*

Figures 13 (*a*) and (*b*) show the displacement thicknesses Δ_μ^* and Δ_θ^*, based on the u and v profiles, respectively. The thickness Δ_μ^* (figure 13*a*) slowly increases from the front towards the rear and from the windward towards the lee side, as was expected for the thickness growth in the downstream direction. But inside the reversed-flow region, an opposite trend is apparent as Δ_μ^* decreases (rather than increases) towards the lee-side symmetry plane as a result of the flattening of the u profile. Figure 13 (*b*) shows that Δ_θ^* varies along the circumferential direction from zero at $\theta = 0$, to a maximum in the middle to zero again at $\theta = 180°$. This result follows from the fact that V varies as $\sin\theta$. Along the meridional direction V is constant, and Δ_θ^* increases downstream. Flow reversal always leads to rapid growth of the boundary layer (of the corresponding component of the flow in the three-dimensional case). This is reflected here in the large increase in Δ_θ^* over the right upper corner in figure 13 (*b*). Note that Δ_μ^* is five times larger than Δ_θ^*, reflecting again the dominance of meridional over circumferential flow. The momentum thicknesses and other details may be found in a recent report by Wang (1974*c*).

3.7. *Repeated calculations*

Because of the exploratory nature of the reversed-flow problem examined here and the unexpected results, the calculation over the afterbody has been repeated carefully with different mesh schemes (figure 3). Over this area, calculations generally required more iterations. The small size of the meridional skin friction $c_{f\mu}$ also contributes to this difficulty in addition to the flow reversal.

At first, the one-step scheme 1 was used for calculations along the circumferential direction from $\theta = 0$ to about 10° beyond the zero-$c_{f\theta}$ line. Scheme 1 then becomes invalid according to the rule of the dependence zone, and scheme 2 was employed to deal with the reversed flow.

Later, scheme 4 (*a*) was developed, and with its advantage of covering a larger zone of dependence, was used to repeat the calculation over the afterbody. The results agreed with those obtained previously. However, small step sizes ($\Delta\theta = 1°$ and 0·5°) were used for both schemes 2 and 4 to avoid difficulty in accounting for the growth of the boundary-layer thickness.

Still later, scheme 4 (*a*) was used to repeat this part of the calculation with additional steps added in the normal (z) direction. This time, however, the computation was carried out more efficiently, and the small step size was no longer required.

As indicated in §3.2, the upper corner of the reversed region, e.g. along

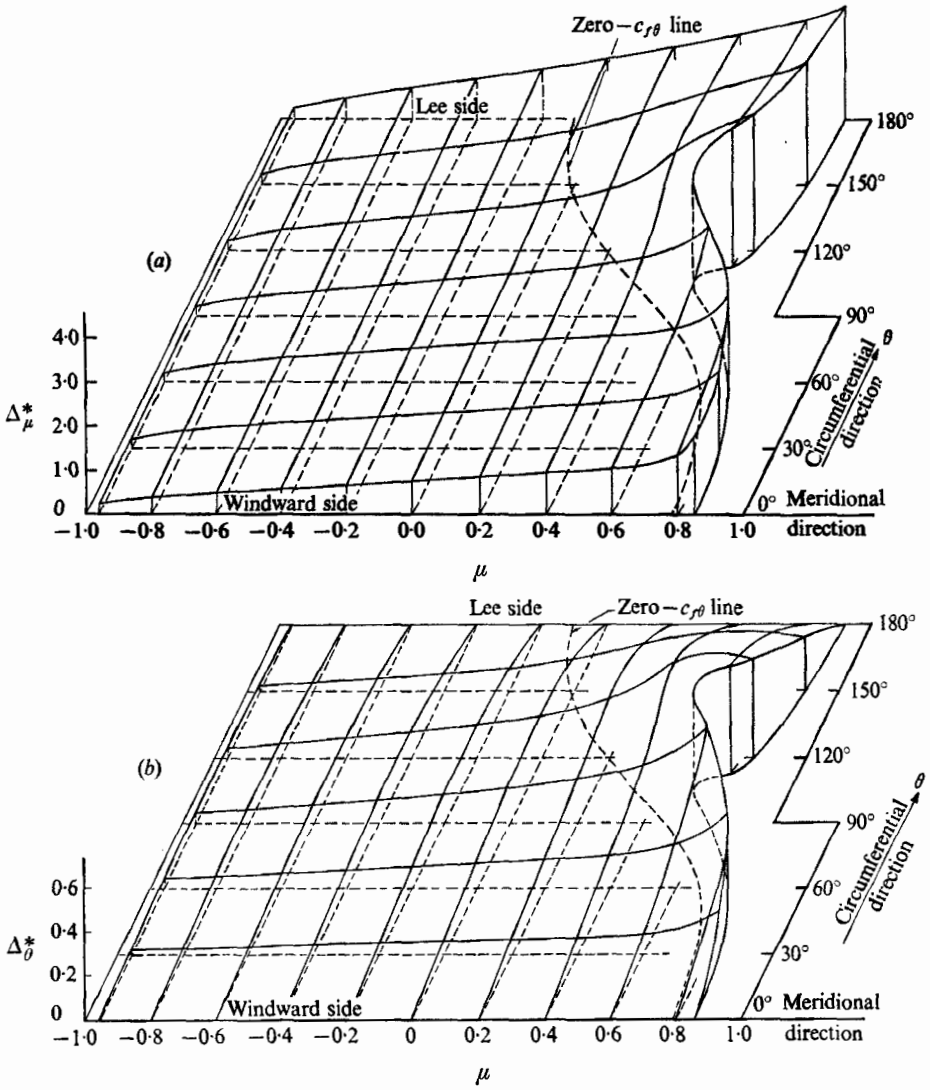

FIGURE 13. Displacement thicknesses. (*a*) Δ^*_μ. (*b*) Δ^*_θ.
Prolate spheroid, thickness ratio = $\frac{1}{4}$, incidence angle = 6°.

$\mu = 0{\cdot}64$, was calculated from $\theta = 180°$ downwards, in contrast to all previous calculations, which proceeded from $\theta = 0$ upwards. Such downward calculation was also extended over the area previously covered by the upward calculation. The agreement of results from such calculations proceeding in two opposing directions in the overlapping area provides an additional check.

4. Conclusions

The three-dimensional laminar boundary layer over a prolate spheroid with $b/a = \frac{1}{4}$ at low incidence was calculated. The results display the general characteristics of a blunt-body boundary layer at low incidence, including the domi-

nance of meridional flow over circumferential flow. More important are the features relating to the circumferential flow reversal: some confirm our early hypotheses, some are new. They include the following.

(i) The reversal of the circumferential flow determines a zero-$c_{f\theta}$ line which does not signify separation.

(ii) The separation line is further downstream of the zero-$c_{f\theta}$ line; situated between these two lines is the circumferentially reversed flow region.

(iii) The existence of a circumferentially reversed region ahead of separation changes the flow structure as usually conceived: the point of vanishing skin friction on the windward symmetry plane is a nodal point and that on the leeward symmetry plane is a saddle point; the usual concept is just the opposite.

(iv) The circumferentially reversed flow considered here can be calculated as a boundary layer so long as the rule of the zones of influence and dependence is obeyed; it is in no way contrary to the basic idea of an initial-value problem.

(v) The coupling between the reversed circumferential flow and the meridional flow leads to an unexpected distribution of $c_{f\mu}$ and an unexpected shape of the separation line.

This work was sponsored by the Air Force Office of Scientific Research, Air Force Systems Command, U.S. Air Force, under AFOSR Contract F44620-70-c-0085. The author is very grateful to Mr William Cooney for his assistance in the early development of this programme, and to Ms Susan Yamamura for her important contributions during the later stage of the effort. The author wishes also to thank the referees for their comments and suggestions for improvement.

REFERENCES

CATHERALL, D. & MANGLER, K. W. 1966 *J. Fluid Mech.* **26**, 163–182.

DWYER, H. A. 1971 *A.I.A.A. Paper*, no. 71-57.

DWYER, H. A. 1974 *Proc. 4th Int. Conf. on Numerical Methods in Fluid Dyn., University of Colorado.*

EICHELBRENNER, E. A. & OUDART, A. 1955 *O.N.E.R.A. Publ.* no. 76.

KITCHENS, C. W., GERBER, N. & SEDNEY, R. 1975 *Ballistic Res. Lab. Rep.* no. 1774.

KRAUSE, E. 1969 *A.I.A.A. J.* **7**, 575–576.

LIN, T. C. & RUBIN, S. G. 1973 *A.I.A.A. J.* **12**, 975–985.

NONWEILER, T. R. F. 1955 In *Incompressible Aerodynamics* (ed. B. Thwaites), pp. 405–406. Oxford University Press.

NONWEILER, T. R. F. 1970 *Nat. Res. Counc. Can. Aero. Rep.* LR-532.

WANG, K. C. 1970 *J. Fluid Mech.* **43**, 187–209.

WANG, K. C. 1972 *A.I.A.A. J.* **10**, 1044–1050.

WANG, K. C. 1974*a* *Proc. Roy. Soc.* A **340**, 33–55.

WANG, K. C. 1974*b* *Phys. Fluids*, **17**, 1381–1385.

WANG, K. C. 1974*c* *Martin Marietta Lab. Rep.* TR-74-14c.

WANG, K. C. 1975 *Martin Marietta Lab. Rep.* (in preparation).

ZAKKAY, V., MIYAZAWA, M. & WANG, C. R. 1974 *N.A.S.A. Contract Rep.* CR-132501.

ZATT, J. A. 1956 *Nat. Aero. Res. Inst. Amst. Rep.* no. 184.